PERGAMON

Journal of Structural Geology 23 (2001) 473–487

JOURNAL OF STRUCTURAL GEOLOGY

www.elsevier.nl/locate/jstrugeo

Comparison of surface slip and focal mechanism slip data along normal faults: an example from the eastern Gulf of Corinth, Greece

Nigel C. Morewood[a,*], Gerald P. Roberts[b]

[a]*Department of Geology, University College Dublin, Belfield, Dublin 4, Ireland*
[b]*The Research School of Geological and Geophysical Sciences, Birkbeck and University College London, Gower Street, London WC1E 6BT, UK*

Received 27 May 2000; accepted 6 June 2000

Abstract

Focal mechanism and surface slip data are used to investigate whether kinematics are similar at depth and at the surface along an active normal fault in the Gulf of Corinth, Greece. We present a new database of slip data from the lateral termination of the South Alkyonides fault segment (SAFS) and the en échelon stepover between it and an adjacent fault, and use published data on surface slip and focal mechanism data pertaining to slip at depth during the 1981 Alkyonides earthquake sequence. The focal mechanisms exhibit similar fault plane orientations and kinematics to those measured at the surface. Within the stepover, both data sets show that contemporaneous c. N–S and c. E–W extension is being accommodated by c. E–W- and c. N–S-oriented normal faults, and the overall deformation is distributed oblate vertical flattening. The deviation of the surface slip direction from 350° increases with distance from the centre of the SAFS. The deviation of the focal mechanism T-axes from 350° fit well with the surface data, implying that the coseismic slip on the SAFS at depths of 7–10 km exhibits a similar kinematic pattern as that observed at the surface. Our results imply that it is critical to know the along-strike position of data on a fault if either focal mechanisms or surface slip are to be used to infer regional strain and stress trajectories.

1. Introduction

Pioneering studies of active normal faults by Paul Hancock suggested that kinematics derived from surface data are similar to those implied by earthquake focal mechanisms (Hancock and Barka, 1987). Hancock and co-workers showed that recently activated or freshly exhumed normal fault planes in the eastern Mediterranean are exposed as smooth polished surfaces that exhibit kinematic indicators ranging from metre-scale corrugations and gutters to centimetre-scale frictional wear striae (Hancock, 1985; Hancock and Barka, 1987; Stewart and Hancock, 1988, 1990, 1991). For the Yavansu fault, western Turkey, they showed that the slip at the surface is parallel to that at depth inferred by the fault plane solution of the 1955 ($M > 7$) earthquake that ruptured a nearby sub-parallel fault (Fig. 1). Many other studies have either shown or assumed the same (e.g. Jackson et al., 1982; Zoback, 1992). The link is important because it unifies the two types of study, and allows both focal mechanism and surface slip data to be used in studies of crustal strain orientations and stress trajectories (e.g. Zoback, 1992; Angelier, 1994, and references therein). For example, many of the results used in producing the World Stress Map are derived from single, composite or an average of several earthquake focal mechanisms and the inversion of fault-slip data measured on Quaternary faults at the surface (Zoback, 1992).

However, recent studies of the patterns of slip measured from striated and corrugated normal faults at the surface reveal a systematic along-strike variation in slip direction along faults, with almost pure dip-slip at fault centres and a large component of oblique-slip at their ends (Roberts, 1996a,b; Roberts and Koukouvelas, 1996; Morewood and Roberts, 1999, 2000; Michetti et al., 2000). To date, such variation has not been revealed by study of focal mechanisms and so it is not known if similar slip patterns occur at depth. Furthermore, the structure and kinematics within the segment boundaries between faults is complex, showing contemporaneous slip in orthogonal directions, resulting in oblate vertical flattening (Morewood and Roberts, 1997, 2000). Again, such complicated strain patterns have not been revealed by focal mechanism studies and it is not known if they continue to depth. If the slip patterns described above do not continue to depth, then slip patterns

* Corresponding author. Tel.: +353-(0)1716-2148; fax: +353-(0)1283-7733.
E-mail address: n.morewood@ucd.ie (N.C. Morewood).

0191-8141/01/$ - see front matter
PII: S0191-8141(00)00126-7

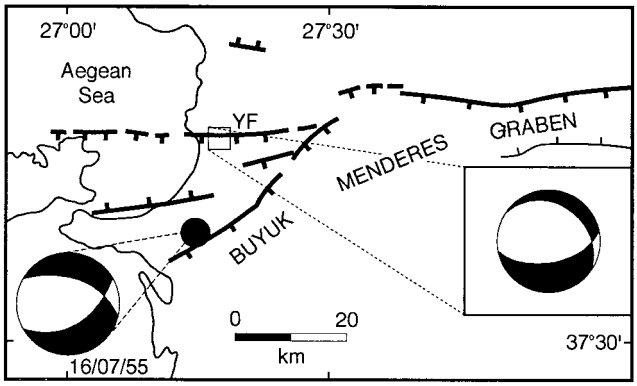

Fig. 1. Map of the western part of the Buyuk Menderes graben, western Turkey, showing the main normal faults and the fault plane solution of the 1955 ($M > 7$) earthquake. The box on the Yavansu fault (YF) indicates the study site of Hancock and Barka (1987), and the inset shows their pseudo-fault plane solution constructed from fault plane and kinematic indicator data from the fault plane exposed at the surface [see Hancock and Barka (1987) for details]. Note the similarity of the fault kinematics implied by the focal mechanism and the surface data. Modified from Hancock and Barka (1987).

at the surface and those from focal mechanisms produced at depth will imply different strain or stress trajectories, despite the fact that slip at the surface and at depth are commonly assumed to be similar.

Two main questions arise. (1) Is the along-strike kinematic variation observed at the surface of normal fault segments also found at depth, where much of the energy release used to produce focal mechanisms arises? (2) Is the complex pattern of deformation observed at the surface within segment boundaries mimicked at depth? We present results and interpretations that go some way towards answering these questions and that should provoke further interest in this topic. We present new data that describe the structure and kinematics within an en échelon stepover (segment boundary) between two normal fault segments in central Greece that were ruptured up to the surface during the 1981 Alkyonides earthquake sequence (Jackson et al., 1982; Ambraseys and Jackson, 1990; Taymaz et al., 1991; Abercrombie et al., 1995; Hubert et al., 1996). We discuss the three-dimensional structure of the en échelon stepover between the two faults and discuss possible links between near-surface faulting and slip at depth, as deduced from fault plane solutions for some of the aftershocks to the 1981 earthquakes (King et al., 1985). We do this by comparing the surface kinematics within the stepover and of one of the major bounding fault segments (the South Alkyonides fault segment, SAFS) with the kinematics implied by aftershocks. In particular, we analyse the variation in slip direction, as deduced from the T-axes of aftershocks, along the strike of the SAFS and compare it to that observed at the surface. Our results imply that it is critical to know the along-strike position of data on a fault if either focal mechanisms or surface slip are to be used to infer regional strain and stress trajectories.

2. Geological and tectonic setting

The Gulf of Alkyonides forms the eastern end of the Gulf of Corinth, central Greece, one of the fastest extending regions of the Earth's continental crust [c. 10 mm/year of N–S extension (Billiris et al., 1991; Clarke et al., 1997)]. Extension across the Gulf of Corinth is accommodated by a system of segmented normal faults (Fig. 2b) (Roberts and Jackson, 1991; Armijo et al., 1996; Roberts, 1996a,b). The Gulf of Alkyonides is bound on its southern shores by the major c. E–W-striking, north-dipping South Alkyonides fault segment (SAFS) (Figs. 2b and 3a) (Roberts and Gawthorpe, 1995; Roberts and Koukouvelas, 1996; Roberts, 1996a,b; Morewood and Roberts, 1999). To the northeast of the Gulf of Alkyonides is the c. E–W-striking, south-dipping Kaparelli fault (KF; Fig. 3a) (Jackson et al., 1982; Hubert et al., 1996).

The SAFS and KF were ruptured up to the surface during the 1981 Alkyonides earthquake sequence (Jackson et al., 1982). Three major events occurred, on the 24th (Ms 6.7) and 25th (Ms 6.4) of February and 4th March (Ms 6.2), and these have been extensively studied (Jackson et al., 1982; King et al., 1985; Ambraseys and Jackson, 1990; Taymaz et al., 1991; Abercrombie et al., 1995; Hubert et al., 1996). The epicentres of the three events were located in and around the Gulf of Alkyonides and correspond to normal faulting accommodating the regional c. N–S extension, consistent with other known earthquakes in the Gulf of Corinth (Fig. 2a) (Jackson et al., 1982; Billiris et al., 1991; Taymaz et al., 1991). In this study, we use the aftershock data of the 1981 earthquakes presented by King et al. (1985). These are discussed in Section 3.

The SAFS comprises a number of fault strands (e.g. Perachora–Pisia–Skinos–Psatha) and has a total surface trace length of c. 35 km (Fig. 3) (Roberts, 1996b; Jackson, 1999; Morewood and Roberts, 1999). Fault-slip data measured above or away from the 1981 surface ruptures show a systematic variation in slip direction along the SAFS, with nearly pure dip-slip at the centre and a large component of along-strike extension at the ends (Roberts, 1996a,b; Morewood and Roberts, 1997, 1999). These striations and corrugations were produced by earthquakes prior to the 1981 events and record the slip pattern along the SAFS over a time period associated with many earthquakes (Roberts, 1996b). A similar, but not identical, converging pattern was measured for the 1981 surface ruptures (Fig. 3a; see Section 5.2) (Jackson et al., 1982). The coseismic throws of the 1981 ruptures were observed to decrease towards the western tip of the SAFS and to the east of Skinos (Jackson et al., 1982). The maximum cumulative throw is 2.5–3.0 km, and occurs in the central portion of the SAFS between Skinos and Alepochori (Fig. 3b) (Myrianthis, 1982; Perissoratis et al., 1986; Roberts, 1996b). The throw is c. 1360 m near Skinos and decreases to c. 20 m near Lake Vouliagmeni, at the western end of the SAFS (Morewood and Roberts, 1999) (Fig. 3b). Similarly, at the eastern end of

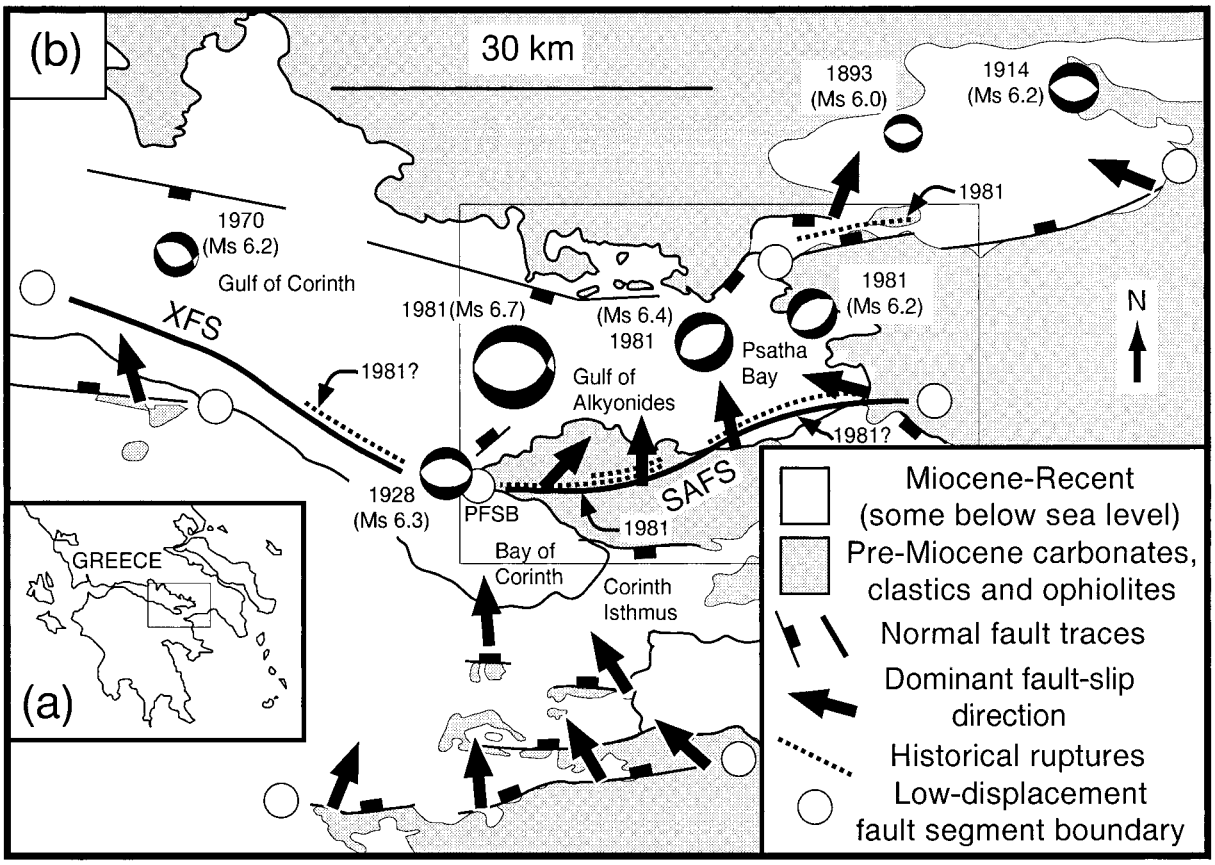

Fig. 2. (a) Location map of Greece. Inset box locates (b). (b) Map showing the segmented normal fault system at the eastern end of the Gulf of Corinth. Thick lines identify the Xylokastro (XFS) and South Alkyonides (SAFS) fault segments. PFSB indicates the position of the Perachora fault segment boundary (see Morewood and Roberts, 1997). Focal mechanisms are shown for all earthquakes >Ms 6.0 since 1893 (from Billiris et al., 1991). Known and suspected surface ruptures are from Jackson et al. (1982), Abercrombie et al. (1995), and Hubert et al. (1996). Dominant fault-slip directions are from Roberts (1996a). Box locates Fig. 3a.

the SAFS, the throw decreases from c. 1.0–1.5 km near Alepochori (Leeder et al., 1991; Armijo et al., 1996) to c. 170 m about 3 km inland of Psatha Bay (Roberts and Gawthorpe, 1995) (Fig. 3b). Surface ruptures produced during the 1981 earthquakes broke only the western half of the SAFS.

The KF comprises three main fault strands, two of which were ruptured in 1981 (Jackson et al., 1982). The two ruptured strands form a left-stepping en échelon geometry (Figs. 2b, 3a and 4a). The third strand of the KF, not ruptured in 1981, is sub-parallel to the others and appears to be the westward continuation of the easternmost strand (Figs. 3a and 4a). The fault strands are clearly expressed at the surface by nearly continuous scarps. Coseismic displacement associated with the 1981 event decreased towards both ends of the eastern strand and towards the eastern end of the western strand (Jackson et al., 1982). The footwall of the northwest strand of the KF reaches c. 600 m and is composed of Mesozoic limestones. The hanging wall of the KF forms a topographic low and contains a maximum of c. 230 m of fluvio-terrestrial deposits of probable Pleistocene age, which dip gently towards the KF (IGME, 1984) and overlie Mesozoic limestones (Fig. 4a). The eastern strand exhibits a footwall composed of Mesozoic limestones, at up to c. 400 m elevation, and an alluvial basin overlying outcropping Mesozoic limestones in its hanging wall (Fig. 4a). Thus, the total throw across the KF is of the order of a few hundred metres.

To the east of the KF is the north-dipping Erithres fault segment (EFS; Fig. 3a). The EF is c. 25 km long, has footwall topography reaching c. 1000 m and bounds the southern margin of a Plio-Pleistocene basin (Fig. 4a) (IGME, 1984; Roberts, 1996a). The EF did not rupture during the 1981 Alkyonides earthquakes (Jackson et al., 1982; King et al., 1985) and its northward dip precludes it from encroaching our area of study at depth. The EF is not considered further in this paper.

3. The aftershocks to the 1981 Alkyonides earthquake sequence

King et al. (1985) report 133 aftershocks, measured between the 7th and 16th of March 1981. Of these events,

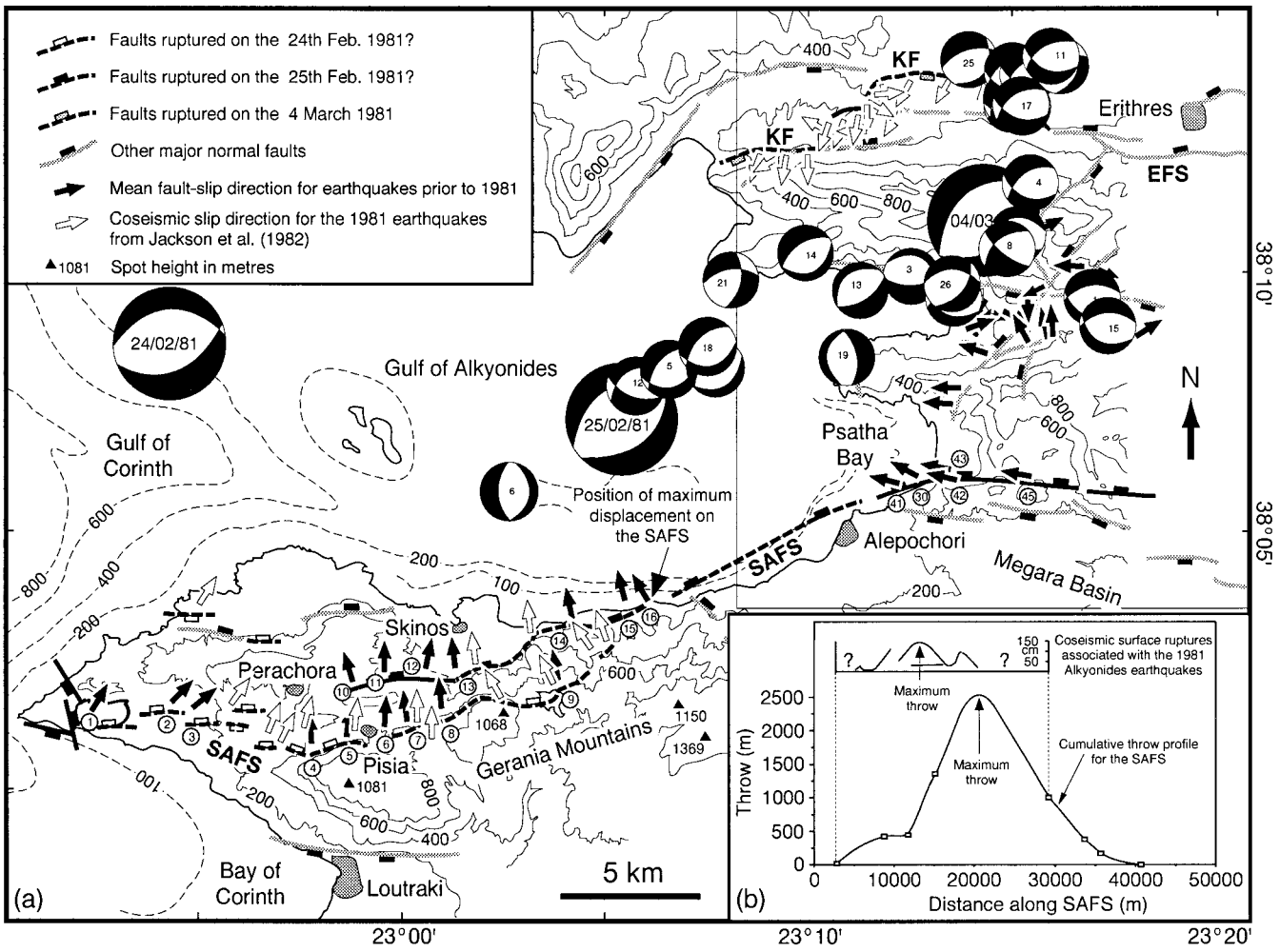

Fig. 3. (a) Map of the Gulf of Alkyonides (located in Fig. 2b) showing the positions of the major faults and focal mechanisms for the 1981 earthquakes and some of the aftershocks. Note the systematic variation in slip direction along the South Alkyonides fault segment (SAFS); dip-slip at the centre and oblique-slip towards the ends of the fault. KF, Kaparelli fault; EFS, Erithres fault segment. The large box at the eastern end of the Gulf locates the area shown in Figs. 4a and 6–8. Details of the focal mechanisms and the surface localities (numbered) are given in Tables 1 and 2, respectively. (b) Throw–distance profile for the SAFS. Throw is at a maximum at the centre [indicated by the arrow on the plot and in (a)], and decreases towards both the western and eastern ends of the SAFS. Also shown is the coseismic throw profile for the 1981 surface ruptures and its position along the SAFS. Note that the 1981 ruptures broke only a portion of the SAFS. Modified after Morewood and Roberts (1999), with additional data presented in this paper and from Jackson et al. (1982), King et al. (1985), and Roberts (1996b).

70 are considered to be very well located and 26 of these provide reliable fault plane solutions (King et al., 1985). The locations and fault plane solutions for these 26 events are shown in Fig. 3a and Table 1, and are thought to be accurate to ±1 km in epicentre and ±2 km in depth (King et al., 1985). In all the figures in this paper, the size of the fault plane solutions represents the error in epicentre of the aftershocks. The majority of the aftershocks lie between the surface traces of the KF and SAFS (Fig. 3a). None of the 26 well-located events, and very few of those less well located, lie within the footwall of the SAFS (also see fig. 1 in King et al., 1985). Reliable depths of the aftershocks range from 3.6 to 13.4 km, although few events are deeper than 10 km (see King et al., 1985). We use the 26 well-located aftershocks to analyse the faulting at depth and compare them to surface data.

4. Field data—the Porto Germano/Psatha Bay area

4.1. Surface geology

A geological map of the Porto Germano/Psatha Bay area, which lies immediately onshore, east of the Gulf of Alkyonides, is shown in Fig. 4a. The area is bound to the north by the KF and to the south by the eastern end of the SAFS. This map is based on published data (IGME, 1971, 1984; Bentham et al., 1991), but we have checked and remapped in the field the nature and geometry of all the lithologies that are offset by faulting and the faults themselves. The studied area, approximately 18 km by 20 km, is dominated by Mesozoic limestones, which are overlain by continental and marine deposits.

The south of the area contains the Plio-Pleistocene

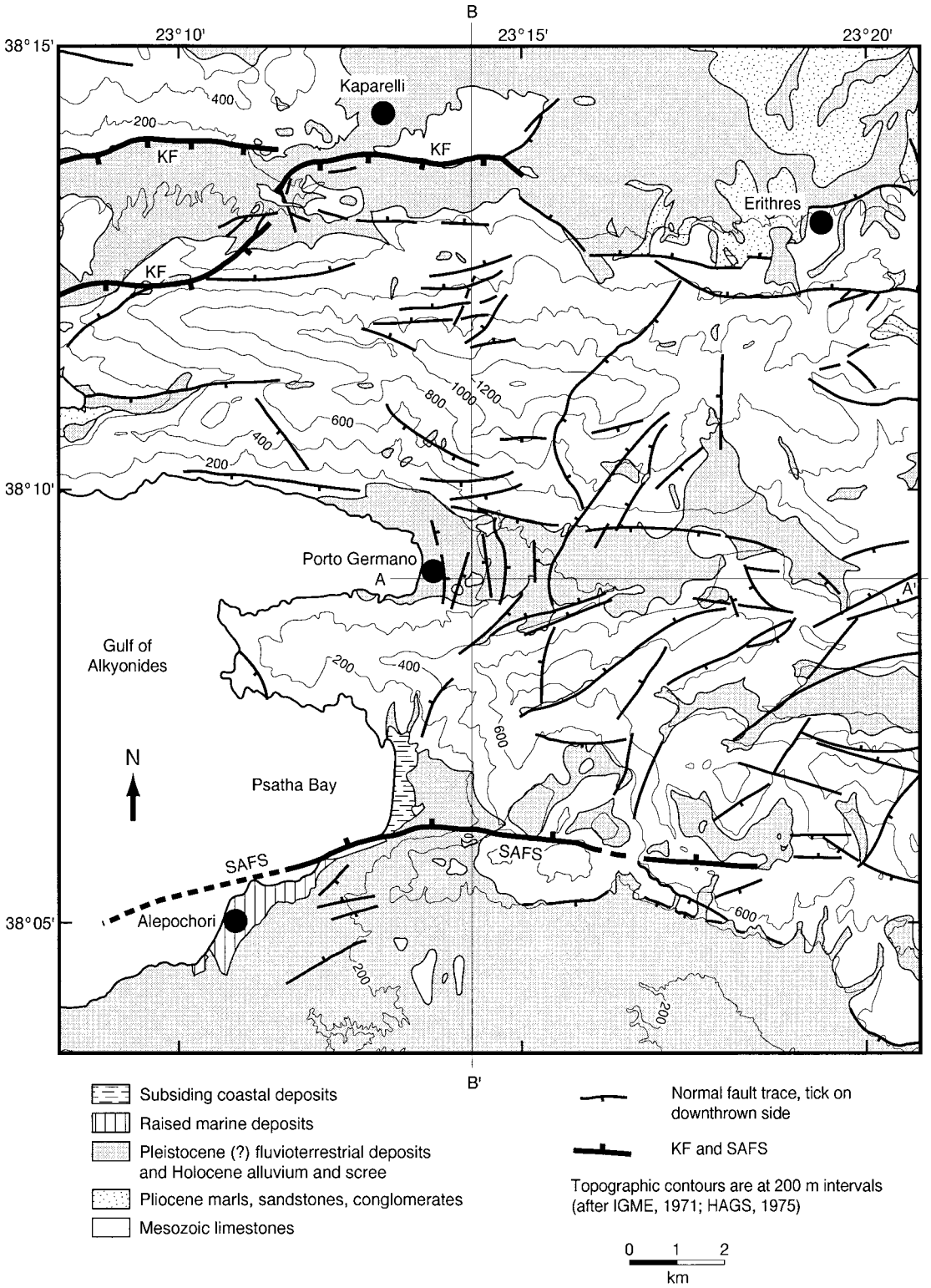

Fig. 4. (a) Geological map of the Porto Germano/Psatha Bay area. KF, Kaparelli fault; SAFS, South Alkyonides fault segment. Lines A–A′ and B–B′ are the lines of cross-sections shown in (b) and (c). (b, c) Cross-sections along the lines indicated in (a), showing the structure of the Porto Germano/Psatha Bay area. Horizontal and vertical scales are equal. Based on IGME (1971, 1984) and Bentham et al. (1991), with additional data collected during this study.

syn-rift deposits of the (now inactive) Megara Basin (Bentham et al., 1991; Leeder et al., 1991; Roberts and Gawthorpe, 1995). Conglomerates of probable alluvial fan and fluvial origin outcrop in areas of relatively low-lying topography in the south, centre and north (Fig. 4). In the north, the conglomerates overlie Pliocene marls, sandstones

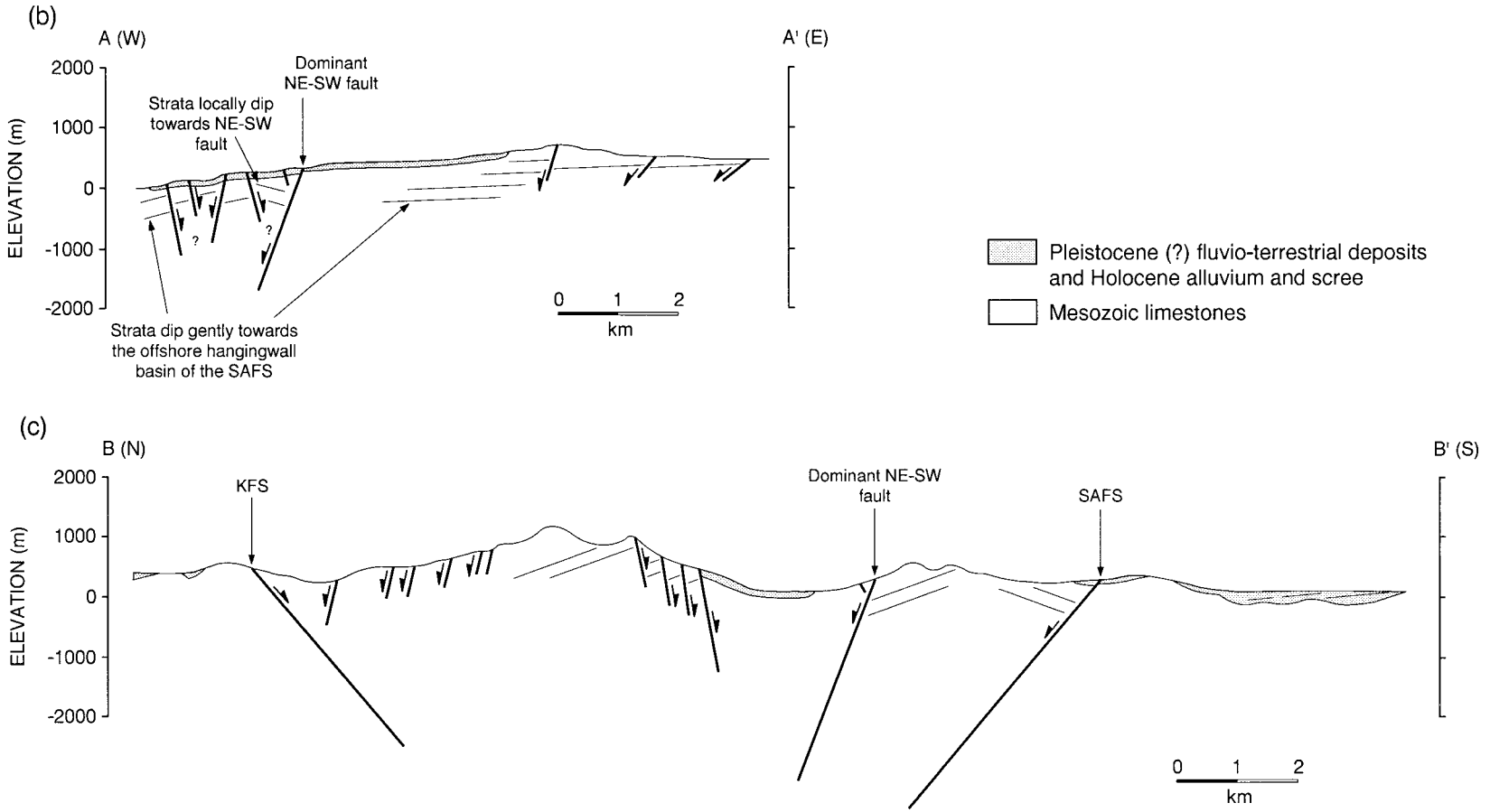

Fig. 4. (*continued*)

Table 1
Summary data table for the 1981 aftershocks used in this study [see King et al. (1985) for further details]

No.	Latitude	Longitude	Depth (km)	T-axis azimuth (degrees)	D350 (degrees)	Distance from SAFS centre (km)
1	38 09.56 N	23 16.96 E	11.37	003-183		
2	38 10.83 N	23 15.11 E	7.30	016-196		
3	38 09.95 N	23 12.54 E	6.36	006-186		
4	38 11.73 N	23 15.46 E	4.86	350-170		
5*	38 08.19 N	23 06.49 E	8.07	329-149	− 021	0.83
6	38 05.54 N	23 02.68 E	8.52	272-092		
7	38 13.41 N	23 14.91 E	9.59	345-165		
8	38 11.04 N	23 14.85 E	11.02	003-183		
9	38 13.67 N	23 14.96 E	8.36	336-156		
10	38 13.88 N	23 14.96 E	9.25	345-165		
11	38 14.18 N	23 15.74 E	10.01	354-174		
12*	38 07.78 N	23 05.85 E	10.36	359-179	009	− 0.09
13*	38 09.65 N	23 11.28 E	7.85	325-145	− 025	0.09
14	38 10.27 N	23 09.92 E	8.06	329-149		
15	38 09.08 N	23 17.36 E	9.67	009-189		
16	38 13.86 N	23 15.27 E	11.78	350-170		
17	38 13.52 N	23 15.01 E	12.24	356-176		
18*	38 08.66 N	23 07.41 E	9.76	331-151	− 019	2.15
19*	38 08.38 N	23 10.90 E	7.09	085-265	− 085	7.15
20*	38 08.36 N	23 07.49 E	10.20	322-142	− 038	2.26
21*	38 09.86 N	23 08.08 E	8.95	317-137	− 033	3.11
22	38 14.04 N	23 16.11 E	12.25	318-138		
23	38 09.50 N	23 13.54 E	9.61	358-178		
24	38 13.37 N	23 15.12 E	8.88	342-162		
25	38 14.15 N	23 14.19 E	13.40	327-147		
26	38 09.77 N	23 13.55 E	8.34	335-155		

Key: No., aftershock number (from King et al., 1985); D350, deviation of slip vector from 350°: positive clockwise, negative anticlockwise of 350°. Distances from the centre of the South Alkyonides fault segment (SAFS) are positive east of the centre and negative west of the centre. Errors are ±1 km for epicentral location and ±2 km for depth (see text and King et al., 1985). *Aftershocks thought to have occurred on the SAFS or on faults closely associated with the SAFS (see text for details).

and conglomerates (IGME, 1971, IGME, 1984). The age of these conglomerates can be crudely estimated through observations of fault displacement. Observations of offset sediments (Leeder et al., 1991) and a thick elastic plate model for fault deformation (Armijo et al., 1996) give a total amount of slip on the SAFS near Alepochori of 1.0–1.5 km. Assuming a constant slip rate of 1.8 mm/year [based on uplifted marine terrace deposits (Armijo et al., 1996)] for the SAFS near Alepochori, we calculate an age of 550–830 ka for the top pre-rift (Louba formation; Bentham et al., 1991). This method estimates a minimum age for the conglomerates because it is assumed that their displacement across the SAFS began immediately after deposition. However, 550–830 ka is consistent with the mid to late Pleistocene age assigned to the conglomerates during previous studies (IGME, 1984; Bentham et al., 1991). Below, we use this age constraint to derive crude estimates for rates of deformation across the faults within the study area.

Around Alepochori, marine terrace deposits are being uplifted in the footwall of the Psatha fault (Leeder et al., 1991) and coastal deposits in Psatha Bay are subsiding in the hanging wall (Roberts and Gawthorpe, 1995) (Fig. 4a). Recent scree and alluvium crop out throughout the area.

4.2. Structure

We have remapped the faults in the Porto Germano/Psatha Bay area using 1:50,000 topographic base maps with 20-m contour intervals to constrain the structure of the area. The results are presented in Fig. 4 and Table 2. The studied area is bound to the south by the eastern end of the north-dipping SAFS and to the north by the KF (Figs. 3a and 4a).

Fault planes are exposed in Mesozoic limestones and Pleistocene continental sediments, and commonly offset Plio-Pleistocene sediments and recent alluvium deposits (Fig. 4). Scarp heights at our localities range between 3 and 20 m (Table 2). Dominant fault trends in the area are c. E–W, N–S, NNE–SSW and NE–SW (Fig. 5). These sets of faults exhibit a mutually cross-cutting relationship; for example, N–S faults cut E–W faults and vice versa. Mean fault dips for each locality vary from 51° to 84° (Table 2). Although we have been unable to map the entire lengths of faults due to incomplete exposure and dense forest, fault lengths at the surface appear to be of the order of 1–10 km.

We note the existence of an NE–SW-oriented fault zone, running from the NE corner of Psatha Bay, in the SW of the area, to c. 4 km SW of the town of Erithres, in the NE of the area (Fig. 4a). This trend is composed mainly

Table 2
Fault orientation, kinematic and deformation rate data for faults within the Porto Germano/Psatha Bay area.

Loc	N	MSD	MSV	FW	HW	SHt (T) (m)	D (m)	H (m)	TR (mm/year)	DR (mm/year)	HR (mm/year)
1	128	196/68	61-274	Mes	sc/al	3.0	3.4	1.7	< 0.01–0.01	< 0.01–0.02	< 0.01–0.01
2	24	220/67	62-287	Mes	sc/al						
3	51	203/79	76-290	Mes	sc/al						
4	64	260/50	48-356	Mes	al	14.0	18.8	12.6	0.02–0.06	0.02–0.09	0.02–0.06
5	32	230/61	59-330	Mes	sc/al	10.0	11.7	6.0	0.01–0.05	0.01–0.05	0.01–0.03
6	68	351/75	67-114	Pt	al/Pt	12.0	13.0	5.1	0.02–0.06	0.02–0.07	0.01–0.02
7	16	074/79	76-177	Mes	Pt						
8	16	193/80	72-246	Mes	Mes						
9	100	221/56	46-270	Mes	sc/al						
10	30	260/54	53-347	Mes	sc	5.5	6.9	4.2	0.01–0.03	0.01–0.03	0.01–0.02
11	17	013/78	65-033	Pt	al	20.0	22.1	9.3	0.02–0.09	0.03–0.10	0.01–0.04
12	20	014/80	77-071	Pt	al	12.0	12.3	2.8	0.02–0.06	0.01–0.06	< 0.01–0.04
13	4	356/69	69-109	Pt	al	20.0	21.4	7.7	0.02–0.09	0.03–0.10	0.01–0.04
14	24	184/83	67-213	Pt	Pt	14.0	15.2	5.9	0.02–0.06	0.02–0.07	0.01–0.03
15	14	348/54	51-059	Mes	sc/al						
23	40	233/84	81-295	Mes	sc						
26	44	091/83	63-131	Mes	Mes						
27	34	320/56	54-063	Mes	Mes						
28	22	171/70	68-272	Mes	al						
29	36	034/51	48-114	Mes	sc						
30	54	244/73	60-298	Mes	sea						
31	30	251/54	49-315	Mes	sc/al						
41	38		− 282	Mes	sea						
42	32		− 285	Mes	Pt						
43	8		− 275	Mes	Pt						
45	10		− 280	Mes	Mes						

Key: Loc, locality; N, number of data; MSD, mean strike/dip of fault plane; MSV, mean slip vector; FW, footwall lithology*; HW, hanging wall lithology*; SHt (T), scarp height (proxy for throw, T**); D, displacement; H, horizontal displacement; TR, throw rate***; DR, displacement rate***; HR, horizontal displacement rate***. *Lithologies: Mes, Mesozoic limestone; Pt, Pleistocene conglomerates; sc, Holocene scree; al, Holocene alluvium. **Minimum estimate of throw (see text). ***Deformation rates are stated for the vertical plane containing the slip-vector azimuth and assume an age for the offset conglomerates of 550–830 ka (see text).

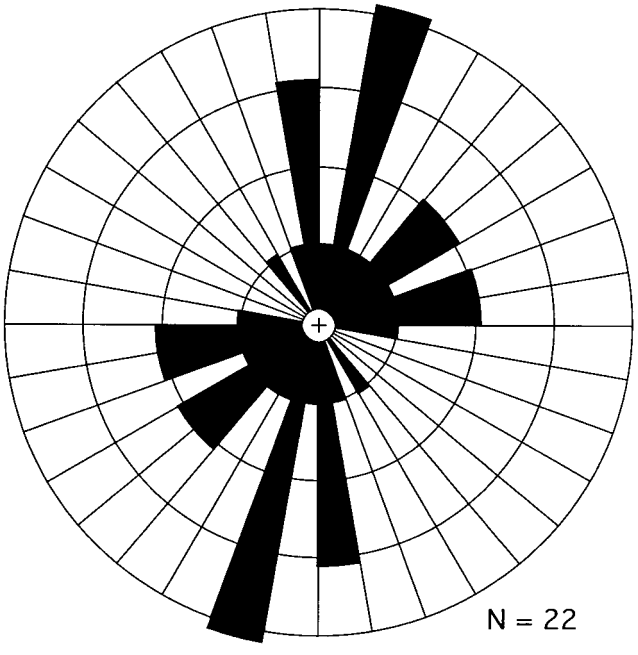

Fig. 5. Rose plot showing the strikes of fault planes from the studied localities (Table 2) within the Porto Germano/Psatha Bay area.

of a c. 8.5-km-long NW-dipping normal fault, which offsets Pleistocene–Recent continental sediments (Fig. 4). The several smaller faults immediately east of Porto Germano also offset Pleistocene–Recent material and are probably hanging wall splays to the main NE–SW-striking fault (Fig. 4b).

The other notable structure in the area is the c. E–W-striking, south-dipping normal fault that bounds the northern edge of the Pleistocene–Holocene fluvio-terrestrial deposits east of Porto Germano (Fig. 4a, c). This fault offsets the fluvio-terrestrial sediments, placing them against Mesozoic limestones, and it is likely that it had some control on the depositional extent of the younger deposits. The c. E–W-striking fault is clearly cut by the NE–SW-striking fault (described above) about 3 km ENE of Porto Germano (Fig. 4a). Both the E–W- and NE–SW-striking faults are active and have influenced the deposition of Holocene sediments in the area.

4.3. Kinematics

Lineations on the faults, such as scratches, grooves and corrugations, were measured at a number of localities (Table 2). The mean slip direction was calculated for each

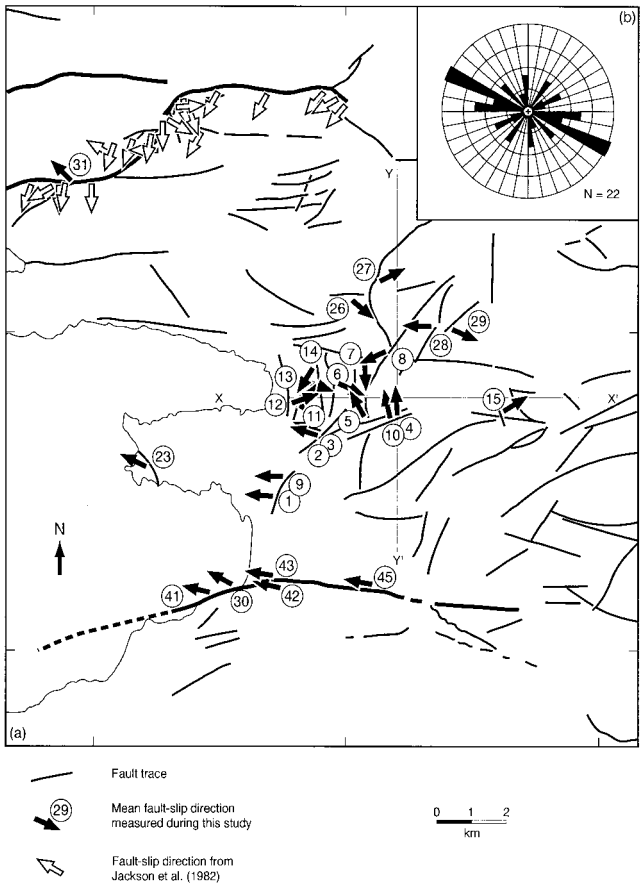

Fig. 6. (a) Map showing the fault kinematics within the Porto Germano/Psatha Bay area. The arrows indicate the mean fault-slip direction for each locality measured from lineations and corrugations on exposed fault planes. Locality details are listed in Table 2. (b) Rose plot showing the variation in fault-slip direction of the studied localities within the area.

locality and plotted in Fig. 6, together with fault-slip data for the 1981 earthquake ruptures from Jackson et al. (1982). Slip is dip-slip to oblique-slip and accommodates c. N–S extension on c. E–W-striking normal faults and c. E–W extension on N–S- and NE–SW-striking normal faults (Fig. 6). A similar pattern of kinematics is observed within the Perachora fault segment boundary, at the western end of the SAFS (Morewood and Roberts, 1997). The plot in Fig. 6b shows a dominance of W- to WNW-directed slip on the faults within the Porto Germano/Psatha Bay area. The significance of this is discussed later.

4.4. Rates of deformation

Assuming an age of 550–830 ka for the faulted conglomerates (calculated in Section 4.1) and using the measured throw or scarp height values, it is possible to calculate rates of deformation across the faults at some of the studied localities. Note that, where possible, the values of throw and displacement given here and in Table 2 are the vertical and down-dip offsets, respectively, of the fluvial–terrestrial conglomerates. Elsewhere, scarp height has been used as a proxy for minimum throw. Using trigonometry, we have calculated the average deformation rates over the last 550–830 ka in the vertical plane containing the slip direction azimuth. The rates of throw, displacement and horizontal motion are shown in Table 2. Ranges of rates of throw are <0.01–0.02 and 0.01–0.09 mm/year, for conglomerates of 830 and 550 ka, respectively. Similarly, ranges of rates of displacement are <0.01–0.03 mm/year (830 ka) to 0.02–0.10 mm/year (550 ka), and those of rates of horizontal motion are <0.01–0.02 mm/year (830 ka) and <0.01–0.06 mm/year (550 ka). We have summed the rates of N–S- and E–W-oriented horizontal displacement along two transects (Y–Y′ and X–X′, respectively, in Fig. 6a). The minimum rate accommodating N–S extension is 0.02–0.06 mm/year and accommodating E–W extension 0.05–0.13 mm/year. These summed rates are minimum estimates, because we have been unable to measure throws across all the faults. Also, more throw data are available for faults accommodating c. E–W extension. However, the summed rates suggest that distributed three-dimensional strain is being accommodated within the en échelon stepover between the KF and the SAFS.

The rates presented here are similar to those measured within the Perachora fault segment boundary, at the western end of the SAFS, where rates of horizontal displacement averaged over the last 125 ka range from 0.01 to 0.14 mm/year and the age of the offset deposits is much better constrained (Morewood and Roberts, 1997). Moreover, the greater amount of throw data and more complete exposure of faults available for Perachora indicate that distributed oblate vertical flattening is occurring (Morewood and Roberts, 1997), similar to that proposed here. Rates derived in the above way for the Porto Germano/Psatha Bay area are, at best, rough approximations compared to those calculated for Perachora. The estimated minimum age means that the actual rates may be lower. Conversely, the maximum throw may be greater than the observed scarp height and therefore the actual rate may be greater than that estimated. Nevertheless, the rates of deformation calculated here provide an indication of the relative fault-slip rates within the Porto Germano/Psatha Bay area, and the similarity with Perachora suggests that they are of the correct order of magnitude.

5. Comparison of field data and the 1981 aftershocks

5.1. Structure and kinematics of the Porto Germano/Psatha Bay area

We have described the surface faulting within the en échelon stepover formed by the KF and the SAFS. However, it is unknown whether such minor faults, within active normal fault systems, are restricted to the near-surface or if they penetrate as continuous or discontinuous fault planes deep into the seismogenic layer. In order to investigate this,

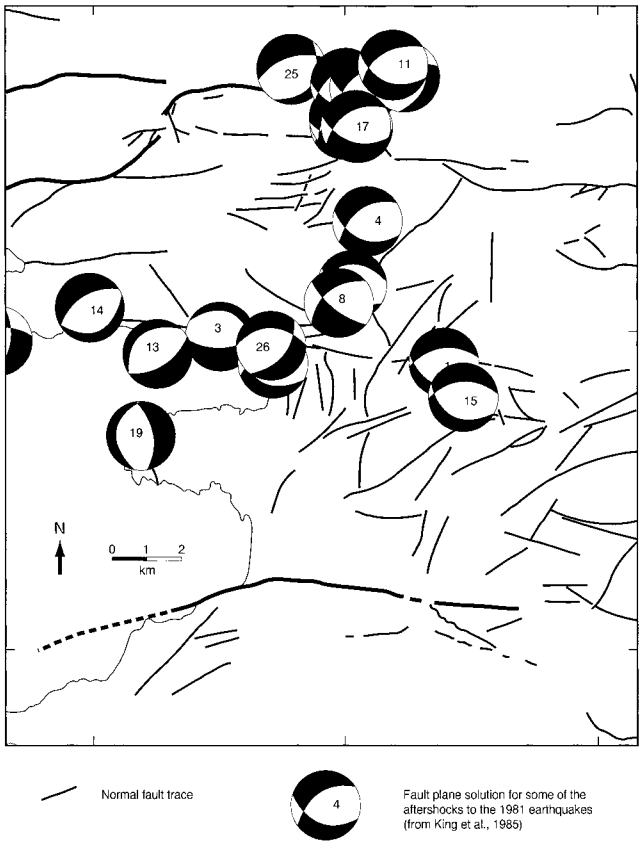

Fig. 7. Map of the Porto Germano/Psatha Bay area with focal mechanisms for some of the 1981 aftershocks. Focal mechanism data are from King et al. (1985) and are summarised in Table 1. The error in epicentral location of the aftershocks is ±1 km and is represented by the size of the symbol.

we have studied the 1981 Alkyonides aftershocks, which occurred at depths of up to c. 13 km (Table 1) (King et al., 1985), within the stepover between the SAFS and KF (Fig. 4a), in combination with structure contour constructions of the main active faults to depth.

The fault plane solutions for the 1981 aftershocks (from King et al., 1985), plotted on our fault map of the Porto Germano/Psatha Bay area, are shown in Fig. 7. On first inspection, it can be seen that similar kinematics are indicated by both the fault plane solutions and the fault-slip at the surface. Both data sets show extension ranging in orientation from c. N–S to c. E–W (Figs. 6 and 7).

The projection to depth of simplified traces of the main SAFS and KF fault planes, both with assumed dips of 50° (Jackson et al., 1982; King et al., 1985), are illustrated in Fig. 8a. The KFS and SAFS intersect at c. 7.5–8.5 km depth (Fig. 8a). There was a concentration of aftershocks at c. 7–8 km depth, which corresponds geographically to the projected intersection of the KF and SAFS (Fig. 8a, Table 1).

Some of the 1981 aftershocks occurred on fault planes that are oblique and in some cases orthogonal to the KF and SAFS (Figs. 3a and 7). In several cases it is unlikely that the events occurred on the KF or SAFS and therefore must have

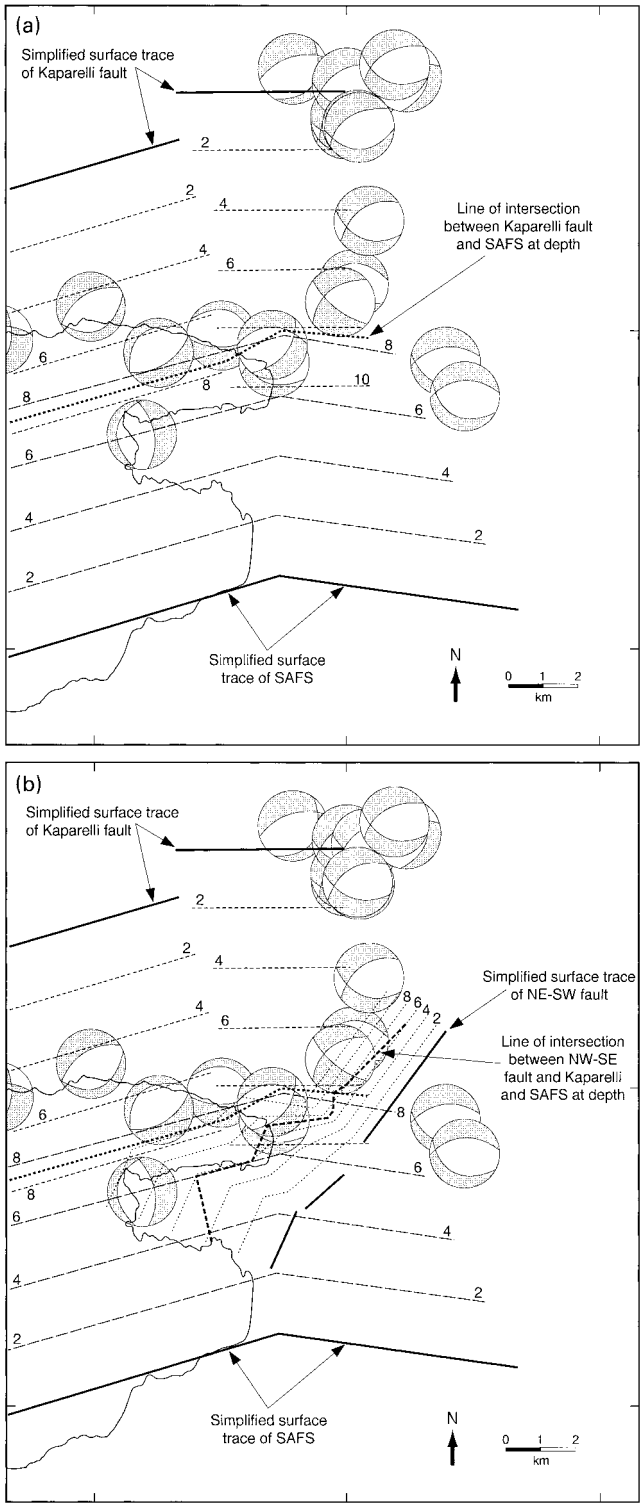

Fig. 8. (a) Structure contours for the Kaparelli fault (KF) and the eastern end of the South Alkyonides fault segment (SAFS). Both faults are assumed to be planar and dip at 50°. Their intersection at about 7.5–8.5 km depth is indicated by the bold, dotted line. (b) Structure contours for the KF, SAFS and the prominent NE–SW-striking fault within the en échelon stepover between the KF and the SAFS. The KF and SAFS have the same parameters as in (a). A 70° dip is used for the NE–SW fault based on field data and the fault is also assumed to be planar. Many of the aftershocks were located at c. 7–8 km depth and were concentrated in the regions of intersection between the faults (bold, dashed line). See text for discussion.

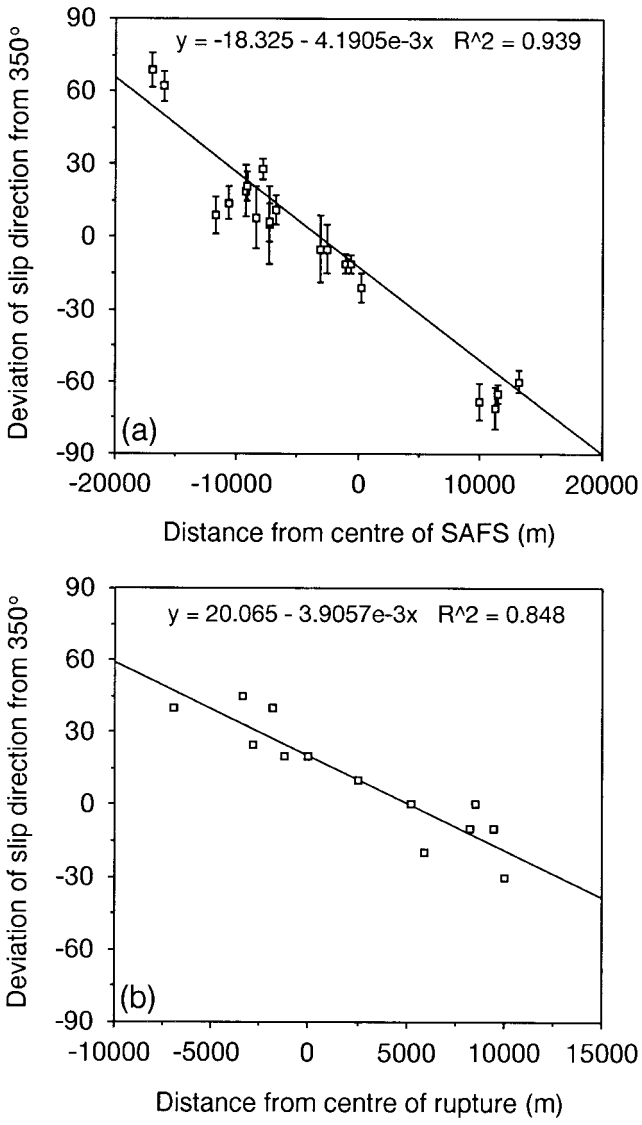

Fig. 9. (a) Deviation of the fault-slip direction from 350° for each field locality (see Fig. 3a and Table 2) plotted as a function of distance from the centre of the South Alkyonides fault segment (SAFS). Localities are accurate to less than 1 km (which is about the size of the symbol) and errors in slip direction are given by the 99% confidence limits for each locality, calculated by Fisher statistics. (b) Deviation of the slip direction of the 1981 surface ruptures plotted as a function of distance from the centre of the rupture (point of maximum coseismic throw; Fig. 3b). Data from Jackson et al. (1982). No errors were ascribed to these data by Jackson et al. (1982). Note that both plots show a good linear correlation but over different along-strike distances. See text for discussion.

ruptured other faults at depth. For example, aftershock 19 occurred on a c. N–S-striking normal fault at a depth of 7.09 ± 2 km (Fig. 7, Table 1). Faults of this orientation are observed at the surface, but have trace lengths of only a few kilometres (Fig. 4a) and may not penetrate to a depth of 7–8 km. Presumably, other faults of similar orientation exist at depth. Aftershock 26 occurred on a c. NE–SW-striking normal fault plane at a depth of 8.34 ± 2 km (Fig. 7, Table 1). It is possible that this ruptured the dominant NE–SW-striking fault within the area (or another fault of similar orientation), because its epicentral location and depth coincide with the projection to depth of the NE–SW fault (Fig. 8b). Even though the nodal planes are oblique to the NE–SW fault, we have weak constraints on the orientation of the fault plane at depth and aftershock 19 may have occurred on such a fault. Similarly, it is also possible that aftershock 26 occurred on the SAFS because of the imprecise constraints on fault geometry at depth. Because of this imprecision, it is also possible that the NE–SW-striking fault strikes nearer to N–S at depth and that it hosted aftershock 19 (Figs. 7 and 8b). It is also apparent from Fig. 8b that the 1981 aftershocks were concentrated at the junction of the NE–SW-striking fault with the KF and SAFS. Thus, the NE–SW fault may have played an important role in restricting aftershock location because very few events were located in its footwall (Figs. 3a, 7 and 8b; also see fig. 1 in King et al., 1985). The cluster of aftershocks at the eastern end of the KF (e.g. aftershocks 11, 17 and 25; Figs. 3a and 7) presumably occurred on faults in the footwall of the KF and are not considered here.

In summary, aftershocks to the 1981 earthquakes are widespread within the en échelon stepover formed by the KF and SAFS, and indicate both c. N–S- and c. E–W-oriented extension on normal faults. The surface fault geometry and kinematics also show contemporaneous c. N–S and c. E–W extension on a number of normal faults. Both sets of data imply distributed deformation (oblate vertical flattening) similar to that observed at the western end of the SAFS. Thus, although we cannot attribute particular aftershocks to particular faults at the surface, we can conclude that the distributed deformation at the surface is similar to that at depth.

5.2. Kinematic variation along-strike of the SAFS

Field studies reveal a characteristic variation in fault-slip direction along-strike of the SAFS (Fig. 3a) (Roberts, 1996a,b; Morewood and Roberts, 1999). Nearly pure dip-slip is observed at the surface of the central portion of the SAFS, which strikes c. E–W near Pisia and Skinos, and c. NE–SW between Skinos and Alepochori (Fig. 3a). At the western and eastern ends of the SAFS, oblique-slip is observed, directed towards the NE and NW, respectively (Fig. 3a). In order to further analyse this variation in slip direction, we have plotted the deviation of the mean slip direction at each locality from a 350° extension direction against distance along-strike of the SAFS (Fig. 9). An extension direction of 350° in used because it is the mean slip direction of the 1981 surface ruptures (Jackson et al., 1982), and is similar to the mean value (345°) for dip-slip earthquake T-axes in the Gulf of Corinth (Jackson et al., 1982; Billiris et al., 1991; Taymaz et al., 1991). The centre of the SAFS is taken to be the point of maximum displacement, about 6 km east of Skinos (Fig. 3) (Roberts, 1996b). The field localities were located in the field on 1:50,000 topographic maps (Roberts, 1996a,b; Morewood and Roberts,

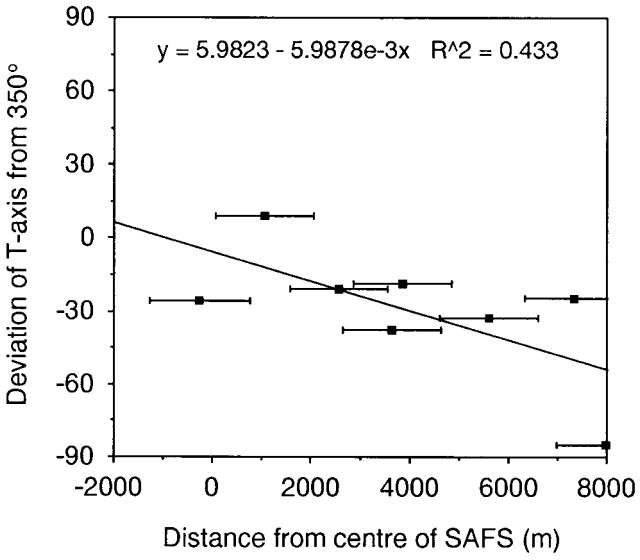

Fig. 10. Deviation of T-axes from 350° for some of the focal mechanisms for the 1981 aftershocks plotted as a function of distance from the centre of the South Alkyonides fault segment (SAFS). Epicentral errors for the aftershocks are ±1 km (King et al., 1985). No errors were ascribed to the T-axes by King et al. (1985). See text for discussion.

1999) and the error in their locations are less than about 1 km, which is about the size of the data points in Figs. 9 and 11. Errors in slip direction are given by the 99% confidence limits for each locality, calculated by Fisher statistics. Errors in epicentral locations of the aftershock data are ±1 km (King et al., 1985).

The deviation of the surface slip direction from 350° shows a good linear correlation ($R^2 = 0.939$) with distance from the centre of the SAFS (Fig. 9a). Intuitively, this is to be expected from the pattern of slip observed at the surface (Fig. 3a). A similar pattern was observed for the surface ruptures produced by the 1981 earthquakes on the SAFS (Fig. 3a) (Jackson et al., 1982). We have plotted the deviation of slip produced by the 1981 ruptures from 350° against distance from the centre of the rupture, where the largest coseismic throws were observed (Jackson et al., 1982), rather than from the centre of the SAFS, where the cumulative throw is greatest. We have chosen to plot these data as a function of distance from the rupture centre because we are interested in the rupture kinematics and the rupture broke only half of the SAFS. A good linear correlation ($R^2 = 0.848$) is observed in Fig. 9b, with deviation from 350° increasing away from the centre of the 1981 rupture. It is clear that the ruptures produced during the 1981 earthquakes exhibit a converging pattern of slip directions similar to that observed along the entire SAFS, but over a shorter distance (Figs. 3 and 9). Because the centre points of the 1981 rupture and the SAFS are different, the two data sets cannot be directly compared. However, it is unlikely that the SAFS grew from ruptures of its entire length (c. 35 km), and growth by the accumulation of many overlapping ruptures explains the converging slip pattern along the SAFS. Indeed, such growth is described by Roberts (1996a,b) and Roberts and Koukouvelas (1996), who suggested that earthquake ruptures must occur in different places along the SAFS in order to produce the observed cumulative throw.

The deviation of the slip direction from 350° increases with distance from the centre of the SAFS, as shown in Fig. 9a. Study of the 1981 aftershocks on the SAFS should reveal if a similar kinematic variation to that observed at the surface occurs at depth. In order to investigate this, we have discarded those aftershocks that are unlikely to have occurred on or close to the SAFS, and plotted the slip direction relative to 350° for the remainder against distance in a manner similar to that described above for the surface slip directions. We have discarded the cluster of aftershocks in the NE of the area, near Kaparelli, because their depth and epicentral location preclude them having occurred on or close to the SAFS (Figs. 7 and 8, Table 2). We have also discarded those aftershocks east of latitude 23°13′ for two reasons. Firstly, east of this latitude, the SAFS decreases rapidly in displacement, from about 200 m at Psatha Bay to having a scarp only a few metres high several kilometres inland (Roberts and Gawthorpe, 1995). We do not expect the low-displacement lateral tip of the SAFS to project to significant depth, that is to the base of the seismogenic layer, and therefore interpret the aftershocks east of latitude 23°13′ to have occurred on other faults (see Section 5.1). We have also discarded aftershocks 3, 6 and 14 because their depth and epicentral location make them unlikely to have occurred on or near to the SAFS (Fig. 8, Table 2). In plotting the data, we use only those pertaining to the aftershocks interpreted to have occurred on the SAFS, or on faults closely associated with the SAFS. Because most of the aftershock fault plane solutions show almost pure dip-slip kinematics (Figs. 3a and 7), the orientation of the T-axes approximates the slip direction and can be compared to the surface slip directions. Note that the limited spatial occurrence of aftershocks means that we have only sampled a small portion of the SAFS, so we expect a less convincing correlation than that given by the surface slip data, because the range of sampled values is only part of the possible full range.

The deviation of the T-axis for each of the aftershocks from 350° plotted against distance from the centre of the SAFS is shown in Fig. 10. As expected, a weak linear correlation is observed ($R^2 = 0.433$), indicating that the deviation of the T-axis from the 350° extension direction increases away from the centre of the SAFS (Fig. 10). Again, we stress that, because of the incomplete spatial coverage of the aftershock data along-strike of the SAFS (Fig. 3a), it is no surprise that the correlation is weak.

In order to assess the relationship between the surface slip and the deeper kinematics, we have combined the focal mechanism and surface slip data. The deviation of the slip directions of our surface localities and the T-axes from the 1981 aftershocks from 350° as a function of distance along the SAFS is shown in Fig. 11. The focal mechanism data fit well with the trend of the surface slip directions and the

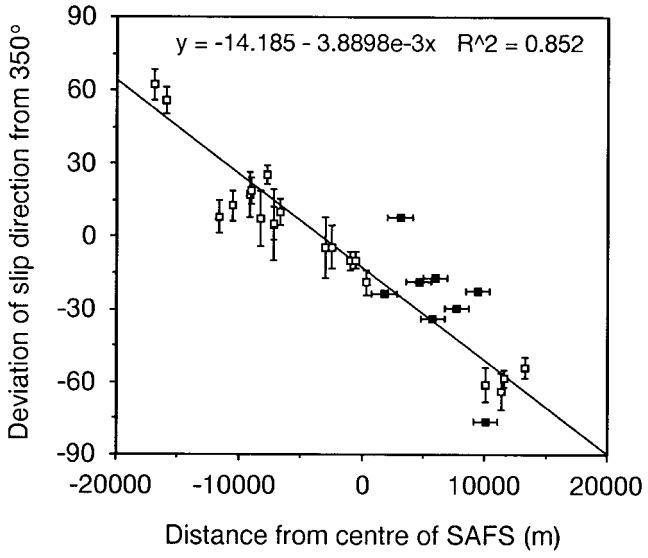

Fig. 11. Plot combining the surface fault-slip and focal mechanism data shown in Figs. 9a and 10. The focal mechanism data fit well with the trend of the surface slip directions and the combined data produce a good linear correlation. See text for discussion.

combined data produce a good linear correlation ($R^2 = 0.852$; Fig. 11). This implies that the coseismic slip on the SAFS at depths of c. 7–10 km exhibits a similar kinematic pattern to that observed at the surface, at least over the limited lateral extent of the fault at depth sampled by the focal mechanism data. It is noteworthy that seven of the eight focal mechanisms plotted in Fig. 11 have T-axes anticlockwise of 350° (Table 1), mimicking the NW-directed slip measured from striated faults at the surface (Fig. 3a). We predict that if future dip-slip earthquakes rupture small portions of the western end of the SAFS at depth, their T-axes will be directed towards the NE (Table 3).

6. Discussion and conclusions

The results of this study have shown that the near-surface structure within and close to the en échelon step between two major active faults (SAFS, KF) is probably representative of the deeper structure (c. 7–8 km). We can infer this because the focal mechanisms for the 1981 aftershocks exhibit similar distributed deformation kinematics and fault plane orientations to those measured at the surface from fault plane kinematic indicators. We do not have sufficient data to determine if the faults exposed at the surface extend to such depths and are the same faults on which some of the aftershocks occurred. However, faults of similar orientation to those observed at the surface exist at depth. Also, it is possible that the more prominent faults, with surface trace lengths of c. 8–10 km (e.g. the NE–SW fault discussed in Section 5.1), do extend to depths of c. 7–8 km. Such faults (e.g. the NE–SW fault) may be important in controlling the distribution of faulting during earthquakes on the adjacent major fault (e.g. SAFS and KF). Only two of the reported aftershocks (King et al., 1985) occurred in the footwall of the NE–SW-striking fault (Figs. 3a, 7 and 8b) and it may be that this fault inhibited the eastward rupture propagation during the 1981 earthquake sequence (Jackson et al., 1982; Abercrombie et al., 1995; Hubert et al., 1996). Faults at a highly oblique angle to the main rift-bounding faults have been recognised in several active normal fault systems worldwide (e.g. Crone and Haller, 1991; dePolo et al., 1991; Machette et al., 1991; Janecke, 1993). These structures often coincide with segment boundaries and have been cited as structures responsible for the termination and hindrance of earthquake ruptures along active normal fault systems (e.g. Machette et al., 1991; Janecke, 1993).

There is a preponderence of W- to WNW-directed slip on the faults within the Porto Germano/Psatha Bay area (Fig. 6). This is probably due to subsidence of the offshore SAFS hanging wall basin stretching the crust at its margins and causing the normal faults to preferentially downthrow towards the basin (King et al., 1985). Similar mechanisms have been proposed for fault-parallel extension at the western end of the SAFS (Morewood and Roberts, 1997) and for normal faults in the northeastern Basin and Range, USA (Anders et al., 1990). Also, a component of lateral slip at the ends of normal faults was suggested by Wu and Bruhn (1994) in their fault growth model based on observations in the South Oquirrh Mountains, Utah. The large NE–SW fault (Section 5.1) appears to accommodate much of the basin-directed slip and is similar to the release faults observed in the Sergipe–Alagoas basin, NE Brazil (Destro, 1995). This component of E–W extension is also reflected in the T-axis orientations of the aftershock focal mechanisms being mainly anticlockwise of 350° on or close to the SAFS.

If along-strike stretching controls fault kinematics together with the regional extension, it will not be a straightforward matter to use focal mechanism data to (1) predict regionally consistent patterns of surface slip: the mainshocks probably average the slip directions at the surface

Table 3
Data pertaining to the three mainshocks of the 1981 Alkyonides earthquake sequence

Date	Centroid depth (km)	Teleseismic slip vector (degrees)	Surface slip vector (degrees)
24 Feb. 1981	12 ± 2	340	350 ± 10
25 Feb. 1981	8 ± 2	324	350 ± 10
24 Mar. 1981	7 ± 3	320	010-030

Centroid depths and teleseismic slip vectors are from Taymaz et al. (1991), and surface slip vectors are from Jackson et al. (1982) and Taymaz et al. (1991).

whilst aftershocks close to the main faults appear to record the variation in slip direction with distance along the fault; (2) infer regional strain and stress orientations, especially if aftershock data are used. Presumably, the aftershocks record the finer detail of kinematic variations along fault planes because they rupture smaller areas than the mainshocks. The same may be true of microseismicity recorded during interseismic periods, but we know of no study which has investigated this. This study shows that it is vital to know where along a fault slip data pertain to if such slip data are to be used to derive regionally consistent strain or stress trajectories. We advocate future, more detailed studies integrating surface and focal mechanism data in order to explore further the kinematic variations within active fault systems.

Acknowledgements

This study was funded by a Birkbeck College Research Studentship (N.C.M.), and NERC GR9/1034 and GR9/02995 and Birkbeck College (G.P.R.). The Benfield Greig Hazard Research Centre provided support. We thank the IGME for permission to conduct field studies, and Simon Baker, Rob Gawthorpe, Richard Phillips and Robin Pilcher for assistance and discussion in the field. Ron Bruhn and Iain Stewart provided constructive comments that improved the paper.

References

Abercrombie, R., Main, I.G., Douglas, A., Burton, P.W., 1995. The nucleation and rupture process of the 1981 Gulf of Corinth earthquakes from deconvolved broad-band data. Geophysical Journal International 120, 393–405.

Ambraseys, N.N., Jackson, J.A., 1990. Seismicity and associated strain of central Greece between 1890 and 1988. Geophysical Journal International 101, 663–708.

Anders, M.H., Geissman, J.W., Sleep, N.H., 1990. Comment on 'Northeastern Basin and Range province active tectonics: An alternative view'. Geology 18, 914–917.

Angelier, J., 1994. Fault slip analysis and palaeostress reconstruction. In: Hancock, P.L. (Ed.), Continental Deformation. Pergamon, Oxford, pp. 53–100.

Armijo, R., Meyer, B., King, G.C.P., Rigo, A., Papanastassiou, D., 1996. Quaternary evolution of the Corinth Rift and its implications for the Late Cenozoic evolution of the Aegean. Geophysical Journal International 126, 11–53.

Bentham, P., Collier, R.E.L., Gawthorpe, R.L., Leeder, M.R., Prosser, S., Stark, C., 1991. Tectono-sedimentary development of an extensional basin: the Neogene Megara Basin, Greece. Journal of the Geological Society of London 148, 923–934.

Billiris, H., Paradissis, G., England, P., Featherstone, W., Parsons, B., Cross, P., Rands, P., Rayson, M., Sellers, P., Ashkenazi, V., Davison, M., Jackson, J., Ambraseys, N., 1991. Geodetic determination of tectonic deformation in central Greece from 1900 to 1988. Nature 350, 124–129.

Clarke, P.J., Davies, R.R., England, P.C., Parsons, B.E., Billiris, H., Paradissis, D., Veis, G., Denys, P.H., Cross, P.A., Ashkenazi, V., Bingley, R., 1997. Geodetic estimate of seismic hazard in the Gulf of Korinthos. Geophysical Research Letters 24, 1303–1306.

Crone, A.J., Haller, K.M., 1991. Segmentation and the coseismic behaviour of Basin and Range normal fault: examples from east-central Idaho and southwestern Montana, U.S.A.. Journal of Structural Geology 13, 151–164.

dePolo, C.M., Clark, D.G., Slemmons, D.B., Ramelli, A.R., 1991. Historical surface faulting in the Basin and Range province, western North America: implications for fault segmentation. Journal of Structural Geology 13, 123–136.

Destro, N., 1995. Release fault: a variety of cross fault in linked extensional fault systems, in the Sergipe–Alagoas Basin, NE Brazil. Journal of Structural Geology 17, 615–629.

Hancock, P.L., 1985. Brittle microtectonics: principles and practice. Journal of Structural Geology 7, 437–457.

Hancock, P.L., Barka, A.A., 1987. Kinematic indicators on active normal faults in western Turkey. Journal of Structural Geology 9, 573–584.

Hubert, A., King, G.C.P., Armijo, R., Meyer, B., Papanastassiou, D., 1996. Fault reactivation, stress interaction and rupture propagation in the 1981 Corinth earthquake sequence. Earth and Planetary Science Letters 142, 573–585.

IGME (Institute of Geology and Mineral Exploration), 1971. Geological map of Greece, Erithrai sheet, scale 1:50,000.

IGME (Institute of Geology and Mineral Exploration), 1984. Geological map of Greece, Kaparellion sheet, scale 1:50,000.

Jackson, J.A., 1999. Fault death: a perspective from actively deforming regions. Journal of Structural Geology 21, 1003–1010.

Jackson, J.A., Gagnepain, J., Houseman, G., King, G.C.P., Papadimitriou, P., Soufleris, C., Virieux, J., 1982. Seismicity, normal faulting, and the geomorphological development of the Gulf of Corinth (Greece): the Corinth earthquakes of February and March 1981. Earth and Planetary Science Letters 57, 377–397.

Janecke, S.U., 1993. Structures in segment boundary zones of the Lost River and Lemhi Faults, East Central Idaho. Journal of Geophysical Research 98, 16223–16238.

King, G.C.P., Ouyang, Z.X., Papadimitriou, P., Deschamps, A., Gagnepain, J., Houseman, G., Jackson, J.A., Soufleris, C., Virieux, J., 1985. The evolution of the Gulf of Corinth (Greece): an aftershock study of the 1981 earthquakes. Geophysical Journal of the Royal Astronomical Society 80, 677–693.

Leeder, M.R., Seger, M.J., Stark, C.P., 1991. Sedimentation and tectonic geomorphology adjacent to major active and inactive normal faults, southern Greece. Journal of the Geological Society of London 148, 331–343.

Machette, M.N., Personius, S.F, Nelson, A.R., Schwartz, D.P., Lund, W.R., 1991. The Wasatch fault zone, Utah—segmentation and history of Holocene earthquakes. Journal of Structural Geology 13, 137–149.

Michetti, A.M., Ferreli, L., Esposito, E., Porfido, S., Blumetti, A., Vittori, E., Serva, L., Roberts, G.P., 2000. Ground effects during the September 9, 1998 $M_L = 5.5$ Lauria Earthquake in southern Italy and the seismic potential of the "aseismic" Pollino region: preliminary report. Seismological Research Letters.

Morewood, N.C., Roberts, G.P., 1997. The geometry, kinematics and rates of deformation in a normal fault segment boundary, central Greece. Geophysical Research Letters 24, 3081–3084.

Morewood, N.C., Roberts, G.P., 1999. Lateral propagation of the surface trace of the South Alkyonides normal fault segment, central Greece: its impact on models of fault growth and displacement–length relationships. Journal of Structural Geology 21, 635–652.

Morewood, N.C., Roberts, G.P., 2000. The geometry, kinematics and rates of deformation within an en échelon normal fault segment boundary, central Italy. Journal of Structural Geology 22, 1027–1047.

Myrianthis, M.L., 1982. Geophysical study of the epicentral area of the Alkyonides Islands Earthquakes, central Greece. Geophysical Institute of Hungary. Geophysical Transactions 28 (2), 5–17.

Perissoratis, C., Mitropoulos, D., Angelopoulos, I., 1986. Marine geological research at the E. Korinthiakos Gulf. In: Special Issue of Geology and Geophysical Research. Institute of Geology and Mineral Exploration, Athens, Greece.

Roberts, G.P., 1996a. Variation in fault-slip directions along active and

segmented normal fault systems. Journal of Structural Geology 18, 835–845.

Roberts, G.P., 1996b. Noncharacteristic normal faulting surface ruptures from the Gulf of Corinth, Greece. Journal of Geophysical Research 101, 25255–25267.

Roberts, G.P., Gawthorpe, R.L., 1995. Strike variation in deformation and diagenesis along segmented normal faults: an example from the eastern Gulf of Corinth, Greece. In: Lambiase, J.J. (Ed.), Hydrocarbon Habitat in Rift Basins. Geological Society Special Publication 80, pp. 57–74.

Roberts, G.P., Koukouvelas, I., 1996. Structural and seismological segmentation of the Gulf of Corinth fault system: implications for models of fault growth. Annalli di Geofisica 39, 619–646.

Roberts, S., Jackson, J., 1991. Active normal faulting in central Greece: an overview. In: Roberts, A.M., Yielding, G., Freeman, B. (Eds.), The Geometry of Normal Faults. Geological Society Special Publication 56, pp. 125–142.

Stewart, I.S., Hancock, P.L., 1988. Normal fault zone evolution and fault scarp degradation in the Aegean region. Basin Research 1, 139–153.

Stewart, I.S., Hancock, P.L., 1990. Brecciation and fracturing within neotectonic normal fault zones in the Aegean region. In: Knipe, R.J., Rutter, E.H. (Eds.), Deformation Mechanisms, Rheology and Tectonics. Geological Society Special Publication 54, pp. 105–110.

Stewart, I.S., Hancock, P.L., 1991. Scales of structural heterogeneity within neotectonic normal fault zones in the Aegean region. In: Hancock, P.L., Yeats, R.S., Sanderson, D.J. (Eds.), Characteristics of Active Faults. Journal of Structural Geology 13, pp. 191–204.

Taymaz, T, Jackson, J.A., McKenzie, D.P., 1991. Active tectonics of the north and central Aegean Sea. Geophysical Journal International 106, 433–490.

Wu, D., Bruhn, R.L., 1994. Geometry and kinematics of active normal faults, South Oquirrh Mountains, Utah: implication for fault growth. Journal of Structural Geology 16, 1061–1075.

Zoback, M.L., 1992. First and second order patterns of stress in the lithosphere: The World Stress Map Project. Journal of Geophysical Research 97, 11703–11728.